Research Square

Preprints are preliminary reports that have not undergone peer review.
They should not be considered conclusive, used to inform clinical practice,
or referenced by the media as validated information.

Design and Nonlinear Force Compensation of an Integrated Knee Distractor for Soft Tissue Balancing in TKA

Enkui Zhang
Changchun University of Science and Technology
He Xu
Changchun University of Science and Technology
Ke Xu
Changchun University of Science and Technology
Xuan Liu
Changchun University of Science and Technology
Jun Hu
Changchun University of Science and Technology
Mingchi Ju
Changchun University of Science and Technology
Tailin Han
hantl@cust.edu.cn
Changchun University of Science and Technology

Article

Keywords: total knee arthroplasty, cantilever beam model, BP neural network, force-error compensation, cubic spline interpolation

Posted Date: November 23rd, 2026

DOI: https://doi.org/10.21203/rs.3.rs-10835825/v1

License: This work is licensed under a Creative Commons Attribution 4.0 International License.
Read Full License

Additional Declarations: No competing interests reported.

Article

Design and Nonlinear Force Compensation of an Integrated Knee Distractor for Soft Tissue Balancing in TKA

Enkui Zhang [1,†], He Xu [1,†], Ke Xu [1], Xuan Liu [1] , Jun Hu [1], Mingchi Ju [1] and Tailin Han [1,*]

1 School of Electronics and Information Engineering, Changchun University of Science and Technology, Changchun 130022, China;
ekuizhang@mails.cust.edu.cn
xh2539859082@163.com
xuke@mails.cust.edu.cn
woliuxuan1@163.com
Jumingchi@mails.cust.edu.cn
hujun@cust.edu.cn
* Correspondence: hantl@cust.edu.cn
† Enkui Zhang and He Xu contributed equally to this work.

Abstract

In total knee arthroplasty (TKA), reliable distractor force measurement is required for quantitative soft-tissue balance assessment. Existing mechanical tensors, passive pressure-sensing trials, and force-controlled systems have improved measurement objectivity, but device deformation, assembly effects, and changing contact conditions can still introduce system-specific error. This study developed an integrated knee distractor with dual-channel independent actuation, force feedback, and distraction-gap detection. Rather than treating the BP neural network as an algorithmic innovation, the study focuses on a device-specific integration of structural design, mechanism-based error characterization, and calibrated nonlinear correction. The load-bearing path was represented by a Γ-shaped cantilever beam model. At a 10 mm distraction gap, the estimated structural-deformation component accounted for an average of 44.20% of the total force discrepancy across the tested loads (range, 32.47%-71.37%), indicating that both structural and non-structural error sources required consideration. A lightweight BP implementation with cubic-spline resampling was then used to model the remaining nonlinear relationship between distraction gap, measured force, and reference load. Under bench-top vertical spacer loading at simulated 0° knee extension, the within-grid assessment yielded a mean absolute error of 0.1671 N, a root mean square error of 0.2020 N, and a maximum error of 0.5074 N; five separately acquired validation conditions produced errors from -0.20 to +0.33 N. These results support the feasibility of the integrated structure-and-calibration workflow within the tested bench conditions, while multi-angle and clinically representative validation remains necessary.

Keywords: total knee arthroplasty; cantilever beam model; BP neural network; force-error compensation; cubic spline interpolation

1. Introduction

As the population ages, the prevalence of arthritis continues to increase. According to the World Health Organization (WHO), China has approximately 120 million patients with arthritis, with an incidence of approximately 13%, and nearly 40% of these patients

require total knee arthroplasty [1]. During TKA, accurate control of soft-tissue tension and distraction force is important for postoperative stability, implant wear, and joint function [2]. Quantitative mechanical assessment is therefore increasingly used to complement surgical experience [3]. Nevertheless, manual distraction and palpation remain subjective, and instrumented measurements can also vary with the device, operator, and loading condition [4,5]. In this setting, the measurement objective is not merely to display a force value, but to obtain reproducible force-gap information that can support medial-lateral and flexion-extension balancing decisions without adding substantial uncertainty to the surgical workflow.

Quantitative soft-tissue assessment in TKA has progressed from mechanical tensors and gap balancers to instrumented distractors, passive pressure-sensing tibial trials, and navigation- or robot-assisted systems [4,15]. The progression also reflects two distinct measurement paradigms. Passive sensor trials record compartmental contact forces generated after component trialing, whereas active tensioning devices apply a controlled distraction load and measure the corresponding gap or stiffness response. The latter can standardize the applied load, but its output depends on the actuator, transmission, contact geometry, and calibration of the complete device rather than the sensor alone. Hasenkamp et al. developed smart instrumentation that measured distraction gap and applied load and enabled estimation of ligament stiffness [31], while Völlner et al. calibrated a knee balancer for in vivo stiffness measurements [21]. More recent work has extended quantitative assessment across the arc of motion using a navigated force-controlled distractor [22], MAKO-assisted gap balancing [23], and independently actuated medial-lateral tension measurement [24]. However, quantitative sensing has not consistently translated into superior clinical outcomes relative to manual balancing [6,32], and measurement repeatability remains affected by sensor behavior, load level, flexion position, and contact conditions [5,18]. These studies establish the feasibility and value of instrumented assessment, but they also leave device-specific measurement error and transparent calibration as relevant engineering problems. They further indicate that improved instrumentation should be evaluated not only by whether it generates a numerical output, but also by how its load path, uncertainty sources, and validation conditions are documented.

Structural analyses of loaded components commonly use cantilever, flexible-beam, or variable-section beam models to describe deflection, strain, and vibration responses [8-11]. These models provide the mechanical basis for examining error in a distractor, but most assume idealized components and boundary conditions. The integrated device studied here has a non-standard Γ-shaped load path in which transverse-beam bending, vertical-beam axial compression, connection rotation, assembly clearance, transmission friction, and contact variation can act simultaneously. Accordingly, the analytical model in this study is used to isolate an interpretable structural component of the measurement discrepancy; it is not presented as a complete stand-alone description of all error sources. In particular, the load is applied at the spacer while the force sensor is located within the drive chain, so the measured response necessarily reflects deformation and loss along the intervening path. The effective moment arm also varies with the working gap, making a device-specific structural representation more informative than direct reuse of a standard uniform-beam calibration.

Neural networks, support vector machines, and related regressors have long been used for nonlinear error compensation in measurement systems [12-14,20,25-27]. A related patent from the authors' institution has also disclosed an ANSYS- and BP-based pressure-error compensation workflow for a knee distractor [33]. Therefore, neither BP regression itself nor its general use for knee-distractor pressure compensation is claimed here as novel. The research question is narrower: whether the experimentally characterized error of a specific dual-channel distractor can be separated into a physically interpretable

structural contribution and a residual multi-source component, and whether a lightweight regression implementation can reduce the residual error within the calibrated bench domain. Existing TKA studies have predominantly emphasized instrument function, intraoperative measurement, or clinical outcomes [6,21-24,31,32], whereas transparent device-level linkage among load-path modeling, quantified structural error, and comparative compensation remains limited.

Accordingly, this study makes three system-level contributions. First, it integrates bilateral independent actuation, synchronous force feedback, and distraction-gap detection in a single TKA distractor, providing measured force and gap as device-specific state variables. Second, it develops a Γ-shaped cantilever representation that decomposes transverse bending, vertical compression, and connection-rotation effects and uses simulation-experiment comparison to estimate the structural share of the observed force discrepancy. Third, it evaluates a lightweight BP implementation, used as an engineering compensation tool rather than a new algorithm, against linear, quadratic, and support-vector regression baselines and then checks the resulting calibration at five separately acquired bench conditions. Together, these elements define the incremental contribution as a mechanism-informed, device-specific design-and-calibration workflow for the tested small-sample setting.

2. Materials and Methods

2.1. Structure of the Knee Joint Surgical Distractor and Error Mechanism Analysis

2.1.1. Structural Design of the Knee Joint Distractor

The structural design of existing knee joint distractors has generally evolved from mechanical scale-based distraction toward three main directions: constant-force control, improved spacer-type balancing tools, and bilateral independently driven tension measurement devices. This progression reflects the growing demands for soft tissue balance assessment during total knee arthroplasty (TKA), shifting from the basic requirement of mechanically distracting the joint gap to reducing uncertainty in manual force application, improving instrument placement and contact conditions, and ultimately enabling independent quantitative measurement of the medial and lateral compartments. For instance, the standard knee balancer described by Völlner et al. [21] features a dual medial-lateral measurement unit, utilizing a knob-spring mechanism for mechanical distraction and scale readout. However, its performance relies on a mechanical spring and scale system, making it susceptible to errors from static calibration offsets and mechanical friction. The knee joint distractor developed by Fan et al. [22] employs a dual-compartment, low-profile design with two built-in antagonistic mechanical actuators, capable of maintaining a quasi-constant distraction force of approximately 90 N on both the medial and lateral sides intraoperatively. Nevertheless, the core functionality of this device remains focused on constant-force distraction and gap acquisition. The improved spacer-type balancing tool utilized by Tsai et al. [23] comprises two flat plates and an offset handle. Gap assessment and tension adjustment are performed by inserting spacers of varying thicknesses into the medial and lateral joint spaces, yet this approach still depends heavily on spacer thickness matching and the surgeon's subjective experience, limiting its quantitative capabilities. The novel knee tensioner proposed by Yang et al. [24] adopts a base tray and dual upward-pushing pedal configuration. It independently actuates the medial and lateral compartments via two motors, while synchronously recording both the gap width and tension values for each compartment. However, accurate measurement with this device requires stable contact between the base and pedals, imposing stringent requirements on intraoperative placement and positioning.

Compared with existing devices that mainly rely on mechanical distraction or constant-force distraction, this study designed an integrated knee joint surgical distractor with dual-channel independent drive and synchronous force and displacement detection. The device is centered on bilateral servo drive chains. Each side consists of a servo motor, mechanical transmission/pushrod assembly, force sensor, displacement sensor, conditioning and acquisition circuit, and MCU control unit. The upper and lower spacers are directly inserted into the knee joint gap and contact the femoral and tibial resection surfaces, forming a load transfer path that is structurally closer to the actual intraoperative working condition. Compared with devices that mainly rely on mechanical scales, spacer thickness matching, or constant-force distraction, this structure can not only achieve independent distraction and synchronous measurement of the medial and lateral compartments, but also simultaneously obtain the control variable, displacement, and measured force, thereby providing more complete state variables for subsequent structural error modeling. Its structure is shown in Figure 1 and Figure 2.

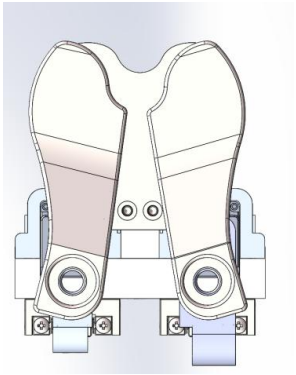


Figure 1. Top view of the knee joint distractor designed in this study. The main bilateral actuation and spacer structures are labeled in the top-view model.

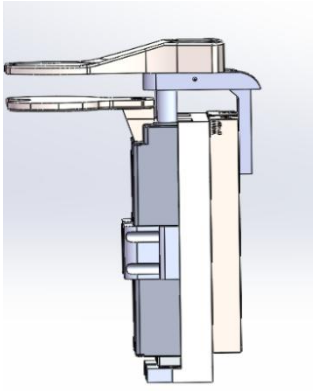


Figure 2. Left view of the knee joint distractor designed in this study. The side-view model shows the relative positions of the spacer, drive mechanism, and measurement unit.

In summary, the first focus of this study is the design of the knee joint force measurement structure itself. Unlike existing instruments that are mostly developed around a single function such as mechanical distraction, spacer matching, or constant-force maintenance, the surgical distractor designed in this study achieves bilateral independent drive and synchronous force and displacement detection. The load transfer path is clear and closer to the actual intraoperative loading state, providing a defined object for subsequent modeling and analysis of its load transfer characteristics, structural deformation, and measurement response.

2.2. "Γ"-Shaped Cantilever Beam Deformation Error Model

For an ideal rigid-body structure, the external load applied to the spacer end should be transmitted to the measurement unit without distortion along the prescribed load transfer path, and the sensor output should be consistent with the target load. However, because the distractor undergoes elastic deformation after loading and is also affected by assembly deviation, transmission clearance, and changes in the contact state, deviations between the measured force output and the target load are unavoidable. Among these factors, the dominant structural error caused by load-induced deformation is directly related to the structural load path and is most suitable for analytical modeling. From the actual structural load path, the external load first acts on the end of the upper spacer, is transmitted through the transverse extension segment to the connection, and is then transmitted through the vertical support segment to the lower support connection. To retain the dominant structural features most closely related to the force measurement error and to establish an analytical error model, the force measurement part is abstracted as a Γ-shaped cantilever beam structure, as shown in Figure 3. The transverse beam corresponds to the upper spacer and its transverse extension, while the vertical beam corresponds to the vertical support connected to the lower support connection. The fixed point is denoted as O; the x-axis extends along the transverse beam from the fixed end (connection point) to the free end (spacer end), with $x = 0$ at the fixed end and $x = L_1$ at the free end. The y-axis extends along the vertical beam from the fixed end (bottom) to the connection point, with $y = 0$ at the fixed end and $y = L_2$ at the connection point. This abstraction is not a simple geometric simplification of the real structure, but a mechanical equivalence based on its main load transfer path. Its purpose is to describe the effects of transverse beam bending, vertical beam axial compression, and additional displacement caused by rotation at the connection on the measurement result.

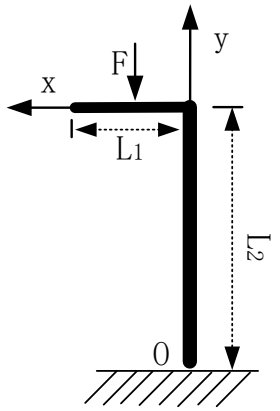


Figure 3. Cantilever beam structure of the distractor. The labels indicate the transverse beam, vertical beam, fixed point, coordinate axes, external load, and effective moment arm used in the mechanical model.

The transverse beam has a mass of $m_1 = 0.177$ kg and a length of $L_1 = 85\ mm$,with an effective moment arm of 25-55 mm. The vertical beam length is $L_2 = 103.5\ mm$. Under the equivalent static loading condition in this study, the force-measurement part of the distractor is simplified as a Γ-shaped beam structure consisting of a transverse beam and a vertical beam. Let L_1 denote the transverse beam length, L_2 denote the vertical beam length, EI_1 denote the equivalent flexural rigidity of the transverse beam, EI_2 denote the equivalent flexural rigidity of the vertical beam, and A_2 denote the equivalent cross-sectional area of the vertical beam. The self-weight of the transverse beam is represented by a uniformly distributed load q, which can be approximated as $q = m_1 g/L_1$. The external load F is assumed to act at a contact position with a horizontal distance a from the connection point, where a is the effective moment arm.

Under the concentrated load F and the uniformly distributed self-weight load q, the vertical deflection of the transverse beam at the contact point can be expressed as Equation (1).

$$w_1(a) = \frac{Fa^3}{3EI_1} + \frac{qa^2(6L_1^2 - 4L_1a + a^2)}{24EI_1} \quad (1)$$

The vertical resultant force transmitted from the transverse beam to the vertical beam is expressed as Equation (2).

$$N_2 = F + qL_1 \quad (2)$$

The axial compression deformation of the vertical beam caused by this resultant force is expressed as Equation (3).

$$\delta_2 = \frac{(F + qL_1)L_2}{EA_2} \quad (3)$$

The end bending moment generated by the transverse beam at the connection is expressed as Equation (4).

$$M_0 = Fa + \frac{qL_1^2}{2} \quad (4)$$

The rotation at the top of the vertical beam caused by this end bending moment is expressed as Equation (5).

$$\theta_2 = \frac{M_0 L_2}{EI_2} \quad (5)$$

The additional vertical displacement at the contact point caused by the rotation at the top of the vertical beam is expressed as Equation (6).

$$\omega_\theta = \mathrm{a}\theta_2 = \frac{a(Fa + \frac{qL_1^2}{2})L_2}{EI_2} \quad (6)$$

Therefore, the total vertical deformation at the contact point of the distractor can be approximately expressed as Equation (7).

$$\omega_{total}(a) = \frac{Fa^3}{3EI_1} + \frac{qa^2(6L_1^2 - 4L_1a + a^2)}{24EI_1} + \frac{(F + qL_1)L_2}{EA_2} + \frac{a(Fa + \frac{qL_1^2}{2})L_2}{EI_2} \quad (7)$$

According to the above equation, the measurement deviation of the distractor after loading is related not only to the external load, but also to the effective moment arm, the bending stiffness of the transverse beam, the axial stiffness of the vertical beam, and the rotation at the connection. Therefore, structural deformation causes deviation between the sensor output and the target load during actual force measurement. The actual force

measurement error still needs to be further analyzed in combination with subsequent simulation and experimental results.

2.3. Simulation Analysis of the Error Model

To verify the ability of the Γ-shaped cantilever beam model to explain the dominant structural error of the knee joint surgical distractor designed in this study, ANSYS was used to simulate the displacement change and stress distribution under loading. The knee joint surgical distractor has two operating modes, namely displacement mode and force control mode. This study focuses on the force measurement error in force control mode when the output displacement is fixed.

The spacer in the knee joint surgical distractor is marked in Figure 4. After resection of the tibial replacement end surface during surgery, the upper and lower spacers are inserted into the knee joint gap and directly contact the femoral and tibial surfaces. Figure 5 shows the structural schematic of the knee joint surgical distractor, where 1 is the upper spacer, 2 is the extension rod, 3 is the flange, 4 is the motion mechanism, 5 is the motor, and 6 is the force sensor. Based on the actual load transfer path, the subsequent simulation analysis model can be further established.

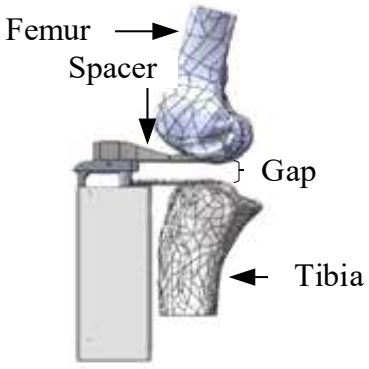


Figure 4. Model of the knee joint surgical distractor. The spacer position used for loading and force transmission is marked in the model.

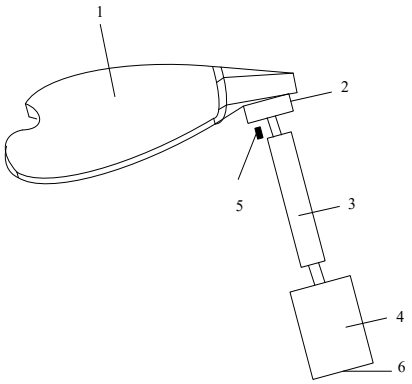


Figure 5. Structural schematic of the surgical distractor : 1-upper spacer; 2-extension rod; 3-flange; 4-motion mechanism; 5-motor; 6-force sensor.

Simulation analysis of the distractor was then performed in ANSYS. First, the geometric model of the knee joint distractor was imported, and basic material parameters of structural steel, including elastic modulus, Poisson's ratio, and density, were defined in the material property settings. The model was then meshed with an overall hexahedral structured mesh. Local mesh refinement was applied to regions with large loads and

stress concentration tendencies, such as the upper spacer and connection joints, to improve calculation accuracy. On this basis, a static analysis condition was established. Fixed constraints were applied to the bottom motor pushrod, a vertical downward load was applied to the upper spacer, and static solution was completed to obtain the displacement change and stress distribution of the knee joint distractor under loading.

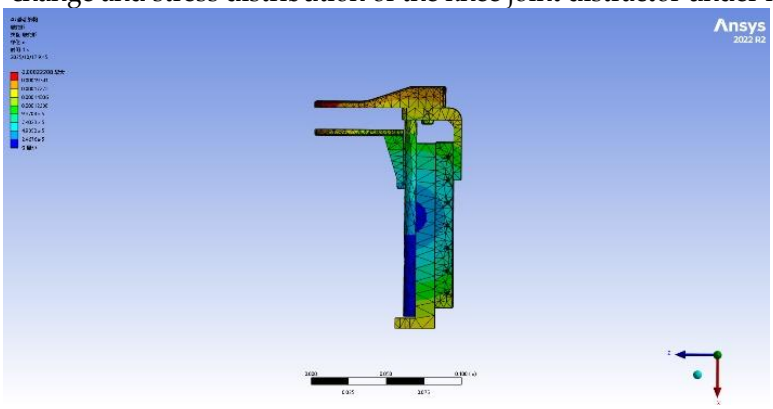


Figure 6. Force model of the Γ-shaped cantilever beam. The arrows indicate the load direction and force-transmission path, and the labels define the equivalent geometric and stiffness parameters.

Taking the working condition of distraction gap $d = 10\,mm$ as an example, Table 1 compares the target load (the known load applied at the spacer position of the surgical distractor), the simulated value (the response force at the sensor position of the surgical distractor obtained by ANSYS simulation), and the measured force (the force value measured by the sensor of the actual surgical distractor):

Table 1. ANSYS simulation and experimental data of the cantilever beam model under different loads at a distraction gap of $d = 10\,mm$.

Target load	20 N	40 N	60 N	80 N	100 N	120 N
Simulation data	15.297 N	35.724 N	55.941 N	75.823 N	95.172 N	115.204 N
Measured force	13.41 N	29.03 N	48.37 N	70.28 N	89.15 N	105.23 N

The comparison between the simulation data and experimental data in Table 1 shows that the simulated values are lower than the target loads, and the measured force values are further lower than the simulated values. If the difference between the target load and the ANSYS simulated value is approximately regarded as the structural deformation error, and the difference between the target load and the measured force is regarded as the total force measurement error, then under the d = 10 mm condition, the structural deformation error accounts for approximately 32.47%-71.37% of the total error, with an average of approximately 44.20%. This indicates that structural deformation is an important source of force measurement error in the distractor, but the experimental error still includes non-structural factors such as assembly deviation, transmission clearance, friction, and changes in the contact state.

On this basis, this study first selected the 0° knee extension position as a typical working condition and conducted the error compensation experiment under the condition that the loading direction on the spacer was approximately perpendicular to the spacer surface. At the same time, different distraction gaps and load levels were set so that the samples covered the main force measurement states within the common working range of the distractor. It should be noted that the experimental validation in this study mainly focused on the equivalent loading condition at 0° extension, and the compensation accuracy at other flexion angles still needs to be verified through multi-angle experiments.

2.4. Design of the Error Compensation System Process

2.4.1. BP Neural Network Structure Design Based on Data Augmentation

To meet the error compensation requirements of the TKA distractor, a dedicated BP neural network error compensation model was constructed in MATLAB R2022a. The training process was divided into two alternating stages around the error compensation objective: forward propagation and backpropagation. In the forward propagation stage, the distraction gap and measured force are input into the network. After layer-by-layer calculation through the input and hidden layers, the compensated force value is output. The mean squared error is used as the objective function to calculate the error of the current compensation model and is used as the accuracy criterion for the output result. In the backpropagation stage, the compensation error is propagated backward from the output layer to the input layer, and the network weights and biases are iteratively updated by minimizing the output error [25].

To adapt to the scenario characteristics of distractor error compensation, the BP neural network was specifically configured. To avoid introducing target load information that is not available in practical application into the model input, the target load was not used as an input variable of the BP neural network. The input variables of the model included the distraction gap and the measured force, and the output variable was the compensated force. The target load was used only as the supervised learning label to calculate the network output error and update the network weights; it did not participate in the model input. Previous studies have shown that a general single-hidden-layer neural network can approximate any continuous function [26]. Increasing the number of hidden layers or hidden neurons increases the network capacity and spatial expressive ability. However, too many hidden layers can lead to overfitting, so multiple adjustment tests should be performed [27]. Therefore, multiple small-scale BP neural network structures were used for candidate training in this study. The candidate structures included single hidden layers with 3, 4, 5, 6, and 8 neurons, and double-hidden-layer structures [6,4], [8,4], and [10,6]. Each structure was trained 30 times, and the models were comprehensively screened according to the mean absolute error, root mean square error, and maximum error on the internal validation set. The network training function was trainlm, the maximum number of iterations was set to 800, the performance function was MSE, and the regularization parameter was set to 0.25 to reduce the risk of overfitting under small-sample conditions. Finally, seven models with better internal validation scores were selected for median ensemble output to reduce prediction fluctuations caused by random initialization of a single model.

The tansig function was selected as the hidden-layer transfer function to satisfy the nonlinear mapping requirements of error compensation, as expressed in Equation (8).

$$f(x) = \frac{1}{1+e^{-2x}} - 1 \quad (8)$$

As a continuously differentiable nonlinear activation function, the tansig function can fit the multi-source coupled nonlinear errors caused by structural deformation, assembly deviation, and contact nonlinearity during force measurement by the distractor, and is suitable for the nonlinear regression prediction scenario in this study. The purelin linear transfer function was selected for the network output layer. This function can directly output linear continuous prediction results without range compression, thereby avoiding additional loss of final force measurement accuracy caused by nonlinear transformation in the output layer.

2.4.2. Error Data Acquisition and Sample Construction

The research object in this study was the force-measurement error of the knee surgical distractor under different distraction-gap conditions. The available data are small-sample, low-

dimensional, structured, and locally smooth with load variation. Cubic spline interpolation was used only as numerical resampling within each observed calibration curve; it was not treated as acquisition of new independent experimental information. Because inappropriate augmentation can distort the observed trend [28,29], interpolation was performed separately for each distraction gap using a piecewise cubic function with continuous first and second derivatives [30]. This procedure increased the sampling density presented to the optimizer while preserving the measured curve shape as closely as possible. Claims of performance outside the calibrated domain were therefore avoided, and separately acquired bench measurements were retained for the practical validation reported in Section 3.3.

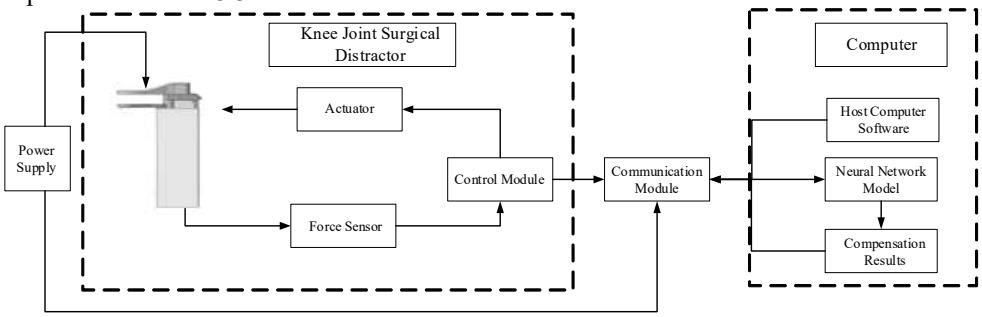


Figure 7. Schematic diagram of the error compensation process. The arrows indicate the sequence of force application, data acquisition, cubic spline interpolation, BP neural network training, and compensated force output.

Figure 7 shows the schematic diagram of the error compensation process. In the experiment, a controllable force source simulating knee joint loading was used to apply loads to the surgical distractor, and the force sensor on the device was used for data acquisition to obtain the original measurement data. First, under different distraction gaps of 10, 15, 20, 25, and 30 mm, target loads of 10-120 N were set for each gap with a target load step of 10 N, yielding 60 groups of original averaged force measurement samples. On this basis, cubic spline interpolation was used to refine the load step from 10 N to 2 N, forming a continuous load grid of 10, 12, 14, ..., 120 N. For each distraction gap condition, 56 augmented samples were obtained, and 280 augmented samples were formed under the five distraction gaps to construct the dataset for network training and testing. To ensure that the test set covered low-, medium-, and high-load ranges and to avoid test points being too close to interpolation endpoints, 18, 32, 46, 60, 74, 88, 100, and 112 N were selected as test load points under each distraction gap condition, forming 40 test samples in total. The remaining samples were used as candidate training samples, of which the load points of 20, 50, 80, and 110 N were used for internal validation, and the other samples were used for network training. The compensation effect of the network was verified through the test set, and visualized error compensation results were finally obtained.

2.4.3. Experimental Setup

The drive and force-measurement unit used in the experiment was the BLACF30-C112 miniature servo electric cylinder (Beijing Inspire Robots Technology Co., Ltd., Beijing, China). The electric cylinder integrates a coreless brushless DC motor, a screw transmission mechanism, a position sensor, a force sensor, and a drive-control system, and it provides closed-loop control of position and push-pull force. Its stroke is 30 mm, the maximum push-pull force is 120 N, the stall push-pull force is 150 N, the maximum self-locking force is 40 N, the repeated positioning accuracy is ±0.01 mm, the communication interface is RS485, and the detection range of the built-in force sensor is -200 to +200 N, with a nominal force-sensor resolution of 0.1 N. Although the nominal resolution of the built-in force sensor was 1 N, the compensated force was obtained as a continuous regression output trained against the reference loads measured by the 0.01 N-resolution digital force

gauge; therefore, the reported residual errors refer to the model-compensated output rather than the raw sensor display resolution. In this study, the built-in force-sensor readings were used as the model input, whereas the reference loads were set and checked using an Aidebao digital push-pull force gauge with a maximum load of 200 N and a resolution of 0.01 N; the force-measurement samples used for model construction were obtained from averaged repeated measurements under each loading condition. The computer configuration was Intel(R) Core(TM) 5 210H (2.20 GHz). Data processing and the error compensation model in the experiment were based on MATLAB R2022a, mainly using its data analysis, signal processing, and neural network toolboxes. The neural network model used was a BP neural network, and its parameters were optimized using MATLAB's training toolbox.

3. Results

3.1. Analysis of Network Training Results

Under distraction gaps of 10 mm, 15 mm, 20 mm, 25 mm, and 30 mm, different target loads were set, and the measured force values from the motor's built-in force sensor were collected. Some samples are shown in Table 2.

Table 2. Original measured force values of the distractor under different distraction gaps and target loads.

Target load / Distraction gap	20 N	40 N	60 N	80 N	100 N
10 mm	13.41	29.03	48.37	70.28	89.15
15 mm	15.29	31.46	52.11	74.33	93.07
20 mm	16.14	33.25	56.49	75.18	95.38
25 mm	16.27	34.32	57.24	75.44	96.12
30 mm	17.35	37.19	58.05	79.41	100.27

It should be noted that because the force measurement error of the distractor is affected by multiple nonlinear factors, the original deviation does not always appear in a single direction. Under small displacement conditions, the measured force is usually lower than the target force. Under larger displacement and high-load conditions, some samples may show local positive errors, namely, the measured force is slightly higher than the target force. For example, when the displacement is 30 mm and the target load is 100 N, the original measured value is 100.27 N, indicating that the system error has clear condition-dependent and nonlinear characteristics.

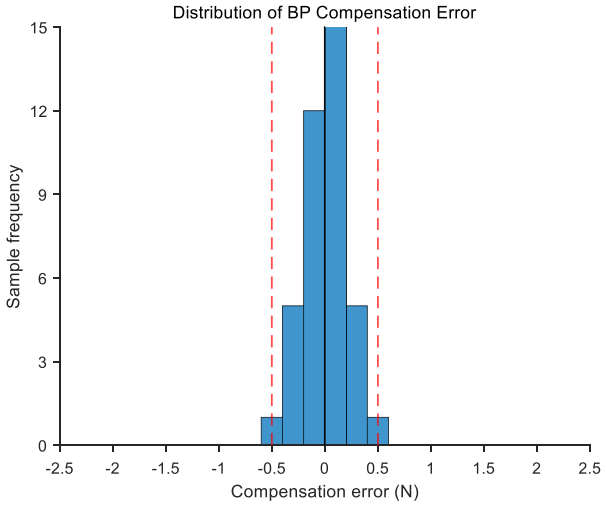


Figure 8. Histogram of compensation error distribution of the BP neural network test set. The red dashed lines indicate the ±0.5 N error limit, and the black solid line indicates zero error.

After training, the error distribution histogram in Figure 8 shows that the errors are mainly concentrated near 0 N and have a relatively compact distribution, indicating that the model has small compensation errors and stable output performance. The red dashed lines in the figure represent the ±0.5 N error limit, and the black solid line represents the zero-error line. In the final test results, the errors of 39 samples were within ±0.5 N, and only one sample slightly exceeded this range, with a maximum error of 0.5074 N. This indicates that the overall compensation stability of the model is good, although further optimization is still needed for individual high-load boundary conditions.

To intuitively verify the effectiveness of the BP neural network compensation method proposed in this study, the uncompensated original force measurement errors were compared with the compensated errors. The comparison results are shown in Figure 9.

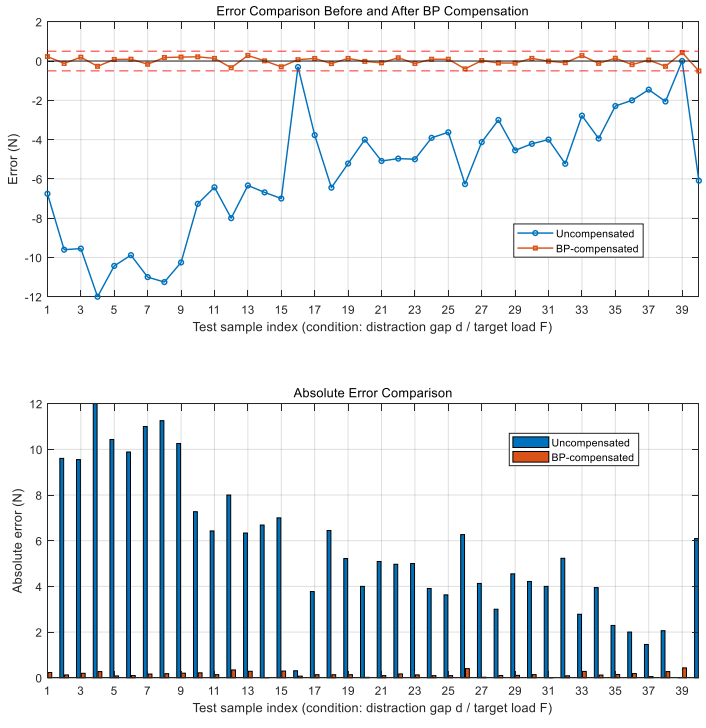


Figure 9. Comparison of test-set errors before and after BP compensation. The curves compare uncompensated and compensated force-measurement errors across the test samples.

The results in Figure 9 show that before compensation, the force measurement errors of the distractor were generally large. Most of the error curve was distributed in the negative-error region and showed clear fluctuations, indicating a considerable systematic deviation between the measured force and the target load. The corresponding absolute errors were also generally high, and most test sample errors were at the level of several newtons. After BP neural network compensation, the error curve converged toward the zero-error line, the overall fluctuation amplitude decreased, and the absolute error was greatly reduced. These results indicate that the method can correct the nonlinear error in the distractor force measurement system and improve the accuracy and stability of the measurement results.

3.2. Comparison of Compensation Effects of Different Methods

To verify the effectiveness of the proposed method, the uncompensated original data, linear least squares method, quadratic least squares method, support vector machine method, and BP neural network method were further compared. As shown in Table 3 and Figure 10, all compensation methods reduced the original force measurement error to some extent. In the uncompensated state, there was a clear deviation between the measured force of the distractor and the target load, with a mean absolute error of 5.6701 N and a root mean square error of 6.4240 N, indicating that the original measurement results could not meet the requirements of high-accuracy force measurement. The linear least squares and quadratic least squares methods improved the error noticeably, and the compensation effect of the quadratic least squares method was slightly better than that of the linear least squares method, indicating that the force measurement error of the distractor has certain nonlinear characteristics. The support vector machine regression model used a Gaussian kernel function, with the kernel scale set to 5, the penalty coefficient set to 10, and the insensitive loss parameter set to 0.2. Under the dataset and parameter settings used in this study, the SVM method reduced the original force measurement error to a certain extent, but its overall compensation effect was weaker than that of the BP neural network. It should be noted that the compensation performance of SVM is closely related to the kernel scale, penalty coefficient, and insensitive loss parameter. In this study, SVM was mainly used as a conventional machine learning comparison method, and large-scale parameter optimization was not performed. Under the dataset and parameter settings used in this study, the BP neural network method achieved the best overall compensation effect, with the mean absolute error and root mean square error decreasing to 0.1671 N and 0.2020 N, respectively. Compared with the uncompensated results, the mean absolute error decreased by approximately 97.05%, indicating that this method can correct the nonlinear deviation in the distractor force measurement system and improve the stability of force measurement output.

Table 3. Error comparison of different compensation methods on the test set.

Method	MAE/N	RMSE/N	Maximum error/N	MAE reduction/%
Uncompensated	5.6701	6.4240	12.0000	—
Linear least squares	1.0881	1.6419	6.1670	80.81
Quadratic least squares	1.0149	1.3345	3.8503	82.10
Support vector machine	1.1619	1.8053	6.6917	79.51
BP neural network	0.1671	0.2020	0.5074	97.05

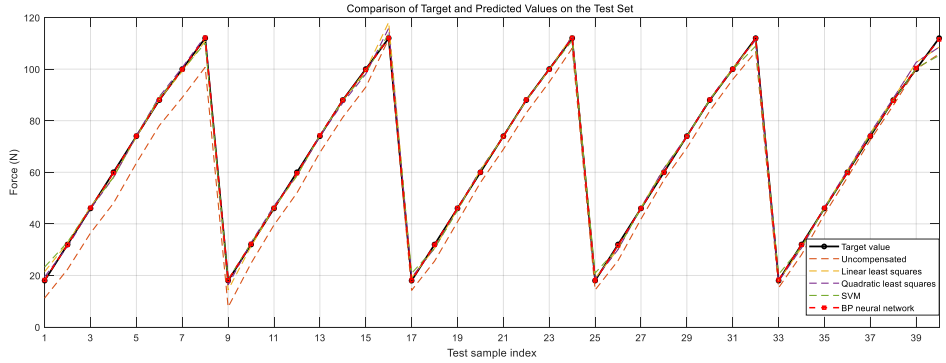


Figure 10. Comparison of compensation outputs of different methods on the test set. The curves compare the target load, original measured force, and compensated outputs from different methods.

3.3. Practical Application Validation

After the compensation experiment, a validation experiment was performed on the test bench. The test bench structure is shown in Figure 11.

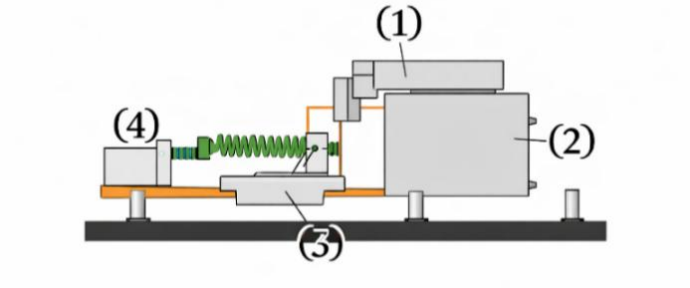


Figure 11. Schematic diagram of the validation test bench：1-surgical distractor body; 2-test bench support; 3-displacement gauge; 4-digital push-pull force gauge.

In Figure 11, (1) is the surgical distractor body, (2) is the test bench supporting the surgical distractor, (3) is the displacement gauge used to measure the displacement of the surgical distractor, and (4) is the digital push-pull force gauge used to measure the force applied to the surgical distractor. The validation results are shown in Figure 12.

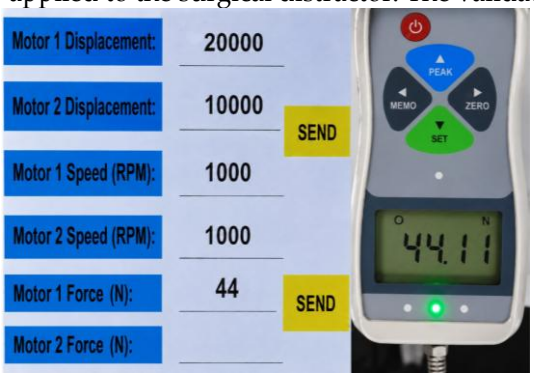


Figure 12. Validation interface and force-gauge reading under the 20 mm distraction gap and 44 N target-load condition.

In the validation experiment, the condition with a gap of 20 mm and a target load of 44 N was tested. The measurement value shown in Figure 12 was 44.11 N, and the difference from the target load of 44 N was 0.11 N, satisfying the ±0.5 N accuracy requirement and indicating that the compensation effect met the expected target. In addition to the above test, several working conditions under different gaps were selected to verify the error compensation results, as shown in Table 4. When the compensated force value is

lower than the target load, the error is recorded as negative. When the compensated force value is higher than the target load, the error is recorded as positive. In Table 4, the target load, compensated force, and error are reported in N, and the value in parentheses is the distraction gap in mm.

Table 4. Validation test results of error compensation.

Target load	Compensated force	Error
32 N (25 mm)	31.8 N	-0.20 N
60 N (30 mm)	60.33 N	+0.33 N
46 N (15 mm)	46.18 N	+0.18 N
44 N (20 mm)	44.11 N	+0.11 N
15 N (10 mm)	14.83 N	-0.17 N

The test results show that the deviation between the target load and the compensated force was small. Under the tested experimental conditions, the compensated force agreed well with the target load, indicating that the proposed method can correct the force-measurement results. After BP neural network compensation, the error between the target load and the compensated force was markedly reduced, and all errors under the independent validation conditions were controlled within the ±0.5 N target. These findings demonstrate that the method can improve the force-measurement accuracy and output stability of the knee joint distractor.

4. Discussion

This study developed an integrated knee surgical distractor for quantitative soft-tissue assessment and evaluated a mechanism-informed nonlinear force-calibration workflow. Relative to mechanical distraction, constant-force devices, and passive sensing trials, the system combines bilateral independent actuation, force feedback, and gap detection in one load path. This integration is the hardware basis for the compensation problem: the measured gap and force are available simultaneously, and the structure being modeled is the same structure used for actuation and measurement.

The simulation-experiment comparison indicates that structural elastic deformation is important but not sufficient to explain the observed force discrepancy. At a 10 mm gap, defining the target-to-simulation difference as the structural component and the target-to-measurement difference as the total discrepancy gave a structural share of 32.47%-71.37%, with an average of approximately 44.20%. The remaining discrepancy is consistent with non-structural influences such as assembly deviation, transmission clearance, friction, and variation in the contact state. This result gives the Γ-shaped model a specific role in the workflow: it identifies and quantifies one physically interpretable component, while the data-driven stage addresses the residual coupled nonlinearity.

Within the tested calibration grid, the BP implementation with cubic-spline resampling reduced the force discrepancy more than the linear, quadratic, and support-vector regression baselines. The within-grid mean absolute error, root mean square error, and maximum error were 0.1671 N, 0.2020 N, and 0.5074 N, respectively, and the five separately acquired validation conditions yielded errors between -0.20 and +0.33 N. These findings support improved output agreement under the specified bench conditions. However, interpolation increases numerical sampling density rather than independent information; consequently, the interpolated test results should be interpreted as within-domain calibration performance, not evidence of broad model generalization.

BP neural-network compensation is an established engineering technique, and the related patent disclosure confirms that applying BP compensation to a knee distractor is not, by itself, a new contribution [33]. The incremental value of the present study should

therefore be interpreted at the system level. Compared with earlier smart instrumentation for simultaneous gap and load measurement [31], navigated force-controlled distraction [22], robot-assisted gap balancing [23], and passive intraoperative pressure sensing [6,18], this work focuses explicitly on the distractor's own load path and measurement discrepancy. It links a Γ-shaped analytical representation to a quantified simulation-experiment error partition and then benchmarks the residual correction using several regression approaches. This positioning distinguishes device-specific mechanism-informed calibration from algorithmic novelty, but it does not imply clinical superiority over existing balancing technologies.

Several limitations should be acknowledged. First, the dataset was obtained under controlled bench loading and did not include patient-specific anatomy, bone-resection morphology, or soft-tissue interaction. Second, the 280 resampled points were derived from 60 original averaged measurements and therefore do not increase the number of independent experimental observations. Third, the five separately acquired validation conditions are insufficient to establish generalization across devices, operators, or load-contact states. Fourth, the present tests used equivalent vertical loading at simulated 0° extension, and the model may require recalibration when the structure, sensor configuration, flexion angle, or contact condition changes. Future work should use independent repeated measurements across the full flexion range and validate the workflow on a physical knee model or cadaveric setup before intraoperative claims are made.

5. Conclusions

This study designed an integrated dual-channel knee surgical distractor and evaluated a mechanism-informed force-calibration workflow that combines a Γ-shaped load-path model with a lightweight BP regression implementation. The central contribution is the system-level linkage of device structure, quantified structural-error analysis, and residual nonlinear calibration; BP regression itself is treated as a mature engineering tool rather than the source of novelty. Under bench-top vertical loading at simulated 0° extension, the within-grid MAE, RMSE, and maximum error were 0.1671 N, 0.2020 N, and 0.5074 N, respectively, while five separately acquired validation conditions produced errors from -0.20 to +0.33 N. These results support feasibility within the tested calibration domain but do not establish clinical effectiveness or cross-condition generalization. Multi-angle testing with independent repeated samples and validation in a physical knee model or cadaveric setting is required before intraoperative application.

Author Contributions

Conceptualization, E.Z. and H.X.; methodology, E.Z., H.X. and T.H.; software, K.X. and X.L.; validation, E.Z., H.X., J.H. and M.J.; formal analysis, E.Z. and H.X.; investigation, E.Z., H.X. and X.L.; resources, J.H. and T.H.; data curation, H.X., K.X. and X.L.; writing—original draft preparation, E.Z. and H.X.; writing—review and editing, E.Z. and H.X.; visualization, E.Z., K.X. and M.J.; supervision, T.H.; project administration, T.H.; funding acquisition, T.H. All authors have read and agreed to the published version of the manuscript.

Funding

This research was funded by the Key R&D Program of Jilin Province Science and Technology Development Plan, grant number 20240302036GX.

Institutional Review Board Statement

Not applicable.

Informed Consent Statement

Not applicable.

Data Availability Statement

The data presented in this study are available on request from the corresponding author.

Conflicts of Interest

The authors declare no conflicts of interest.

References

1. Jin, H.Z.; Wang, Y.; Bai, H.H.; et al. Research progress on perioperative management of total knee arthroplasty for knee osteoarthritis. Chin. J. Surg. Integr. Tradit. West. Med. 2024, 30, 144–149. https://doi.org/10.3969/j.issn.1007-6948.2024.01.029. (In Chinese).
2. Putman, S.; Boureau, F.; Girard, J.; Migaud, H.; Pasquier, G. Patellar complications after total knee arthroplasty. Orthop. Traumatol. Surg. Res. 2019, 105, S43–S51. https://doi.org/10.1016/j.otsr.2018.04.028.
3. Becker, R.; Voss, M.; Lettner, J.; et al. Mean distraction force applied in tension-controlled ligament-balanced total knee arthroplasty: A systematic review and meta-analysis. Knee Surg. Sports Traumatol. Arthrosc. 2025, 33, 2498–2526. https://doi.org/10.1002/ksa.12629.
4. Wu, X.D.; Zhang, Y.; Ma, Z.; et al. From empirical to analytical: Soft-tissue tension gauging in total knee arthroplasty. Knee Surg. Relat. Res. 2025, 37, 40. https://doi.org/10.1186/s43019-025-00287-0.
5. Zhao, R.; Liu, Y.; Tian, H. Accuracy of soft tissue balancing in total knee arthroplasty using surgeon-defined assessment versus a gap-balancer or electronic sensor. J. Orthop. Surg. Res. 2021, 16, 305. https://doi.org/10.1186/s13018-021-02439-w.
6. Sava, M.P.; Hara, H.; Alexandra, L.; et al. Verasense sensor-assisted total knee arthroplasty showed no difference in range of motion, reoperation rate or functional outcomes when compared to manually balanced total knee arthroplasty: A systematic review. Knee Surg. Sports Traumatol. Arthrosc. 2023, 31, 1851–1858. https://doi.org/10.1007/s00167-023-07352-9.
7. Al-Nasser, S.; Noroozi, S.; Harvey, A.; et al. Exploring the performance of an artificial intelligence-based load sensor for total knee replacements. Sensors 2024, 24, 585, https://doi.org/10.3390/s24020585.
8. Sargent, B.S.; Ynchausti, C.R.; Nelson, T.G.; Howell, L.L. The mixed-body model: A method for predicting large deflections in stepped cantilever beams. J. Mech. Robot. 2022, 14, 041001. https://doi.org/10.1115/1.4053376.
9. Zhao, R.; Song, Q.Z.; Chen, H.Y.; Li, X.D.; Gu, Y.S. Analysis and Verification of Self-weight Influence on Large Deformation of Highly Flexible Cantilever Beams. Mech. Sci. Technol. Aerosp. Eng. 2026, 45, 345–350, https://doi.org/10.13433/j.cnki.1003-8728.20250111. (In Chinese).
10. Wang, Q. Study on dynamic strain measurement technology based on variable-section cantilever beams. Master's Thesis, Zhejiang Sci-Tech University, Hangzhou, China, 2023, https://doi.org/10.27786/d.cnki.gzjlg.2023.001705. (In Chinese).
11. Pham, P.T.; Nguyen, Q.C.; Yoon, M.; Hong, K.S. Vibration control of a nonlinear cantilever beam operating in the 3D space. Sci. Rep. 2022, 12, 13811. https://doi.org/10.1038/s41598-022-16973-y.
12. Liang, J.; Feng, S.; Zhen, M.J.; et al. Comprehensive error compensation method for coordinate measuring machine based on geometric error model and neural network. Chin. J. Sci. Instrum. 2025, 46, 150–159, https://doi.org/10.19650/j.cnki.cjsi.J2513839. (In Chinese).
13. Liu, Y.; Ma, X.T.; Feng, Z.Q.; et al. Stiffness prediction-neural network based error compensation for attitude adjustment platform. Opt. Precis. Eng. 2022, 30, 3139–3158. (In Chinese).
14. Lei, Y.; Wang, L.; He, Y.P.; et al. Research on error analysis and compensation technology in high-precision geometric measurement. Instrument Users 2025, 32, 36–38. (In Chinese).
15. Park, C.H.; Song, S.J. Sensor-assisted total knee arthroplasty: A narrative review. Clin. Orthop. Surg. 2021, 13, 1–9. https://doi.org/10.4055/cios20034.
16. Wang, B.; Costa-Castello, R.; Na, J.; de la Torre, O.; Escaler, X. Modeling and adaptive parameter estimation for a piezoelectric cantilever beam. IEEE Trans. Circuits Syst. I Regul. Pap. 2023, 70, 481–491. https://doi.org/10.1109/TCSI.2022.3218189.
17. Song, H.; Shan, X.; Zhang, L.; et al. Research on identification and active vibration control of cantilever structure based on NARX neural network. Mech. Syst. Signal Process. 2022, 171, 108872, https://doi.org/10.1016/j.ymssp.2022.108872.

18. Fary, C.; Mckenzie, D.; Steiger, R. Reproducibility of an Intraoperative Pressure Sensor in Total Knee Replacement. Sensors 2021, 21, 7679, https://doi.org/10.3390/s21227679.
19. Wang, F.X.; Wu, Z.Y.; Lin, Q.H.; et al. Novel force measurement system for soft tissue balance in total knee arthroplasty based on flexible pressure sensor arrays. Adv. Intell. Syst. 2022, 4, 2100156, https://doi.org/10.1002/aisy.202100156.
20. Li, X.H.; Leng, Y. Error compensation technology of hemispherical resonator gyroscopes based on BP neural networks. Opt. Optoelectron. Technol. 2026, 24, 54–60, https://doi.org/10.19519/j.cnki.1672-3392.2026.01.004. (In Chinese).
21. Völlner, F.; Weber, T.; Weber, M.; et al. A simple method for determining ligament stiffness during total knee arthroplasty in vivo. Sci. Rep. 2019, 9, 5261, https://doi.org/10.1038/s41598-019-41732-x.
22. Fan, W.; Laurent, A.; Amaury, J.; et al. Gap balancing throughout the arc of motion with navigated TKA and a novel force-controlled distractor: A review of the first 273 cases. J. Arthroplast. 2023, 38, S246–S252. https://doi.org/10.1016/j.arth.2023.03.011.
23. Tsai, K.H.; Bao, Z.; Wu, D.; et al. A new gap balancing technique with functional alignment in total knee arthroplasty using the MAKO robotic arm system: a preliminary study. BMC Surg. 2024, 24, 232, https://doi.org/10.1186/s12893-024-02524-x.
24. Yang, D.; Zhao, Y.; Wang, Z.; et al. Soft tissue elasticity in total knee arthroplasty: An in vivo quantitative analysis. Clin. Biomech. 2024, 120, 106335, https://doi.org/10.1016/j.clinbiomech.2024.106335.
25. Kim, G.; Bak, Y. Forward and Backpropagation-Based Artificial Neural Network Modeling Method for Power Conversion System. Electronics 2025, 14, 4718, https://doi.org/10.3390/electronics14234718.
26. Lewicki, G.; Marino, G. Approximation by superpositions of a sigmoidal function. Z. Anal. Anwend. 2003, 22, 463–470. https://doi.org/10.4171/ZAA/1156.
27. Ding, H.H.; Shao, T.T.; Qiao, X. Error compensation for small-angle well-deviation azimuth based on BP neural networks. Electron. Sci. Technol. 2022, 35, 33–37, https://doi.org/10.16180/j.cnki.issn1007-7820.2022.05.006. (In Chinese).
28. Garcea, F.; Serra, A.; Lamberti, F.; et al. Data augmentation for medical imaging: A systematic literature review. Comput. Biol. Med. 2023, 152, 106391, https://doi.org/10.1016/j.compbiomed.2022.106391.
29. Iglesias, G.; Talavera, E.; González-Prieto, Á.; Mozo, A.; Gómez-Canaval, S. Data augmentation techniques in time series domain: A survey and taxonomy. Neural Comput. Appl. 2023, 35, 10123–10145. https://doi.org/10.1007/s00521-023-08459-3.
30. Sun, M.; Lan, L.; Zhu, C.-G.; Lei, F. Cubic spline interpolation with optimal end conditions. J. Comput. Appl. Math. 2023, 425, 115039. https://doi.org/10.1016/j.cam.2022.115039.
31. Hasenkamp, W.; Villard, J.; Delaloye, J.R.; Arami, A.; Bertsch, A.; Jolles, B.M.; Aminian, K.; Renaud, P. Smart instrumentation for determination of ligament stiffness and ligament balance in total knee arthroplasty. Med. Eng. Phys. 2014, 36, 721-725. https://doi.org/10.1016/j.medengphy.2013.12.001.
32. Sun, C.; Zhao, Z.; Lee, W.G.; Ma, Q.; Zhang, X.; Zhu, J.; Cai, X. Sensor-guided gap balance versus manual gap balance in primary total knee arthroplasty: A meta-analysis. J. Orthop. Surg. Res. 2022, 17, 243. https://doi.org/10.1186/s13018-022-03129-x.
33. Changchun University of Science and Technology. Pressure error compensation method for knee joint spreader. Chinese Patent CN119885486A, 25 April 2025.